Schoettle-Greene, P., et al., 2020, Uplift and exhumation in Haida Gwaii driven by terrane translation and transpression along the southern Queen Charlotte fault, Canada: Geology, v. 48, https://doi.org/10.1130/G47364.1

Data Repository for:

Uplift and exhumation in Haida Gwaii driven by terrane translation and transpression along the southern Queen Charlotte Fault

Philip Schoettle-Greene, Alison R. Duvall, Ann Blythe, Eric Morley, William Matthews, Sean R. LaHusen.

Contents:

1. Thermochronometry methods

Sampling and Mineral Separation

We collected 20 bedrock samples from across the archipelago of Haida Gwaii on two separate occasions in 2016 and 2017. Samples with the prefix CD were collected in the summer of 2016 by C. Dorsey from the University of Calgary. Samples with the prefix HG were collected in the summer of 2017 by P. Schoettle-Greene and S. R. Lahusen from the University of Washington. Sample BARRY was collected by L. Nykolaishen from the Geological Survey of Canada. Samples were excavated from >5cm depth so as to avoid possible reheating from forest fire and lightning strike. HG and BARRY apatite and zircons were separated at Geosep services in Moscow, Idaho, using standard magnetic and heavy liquid techniques. Mineral separation of CD samples was performed at the University of Calgary using standard magnetic and heavy liquid techniques.

(U-Th)/He Thermochronometry

Individual apatite and zircon grains were handpicked at the University of Washington and University of Calgary. P. Schoettle-Greene picked HG and BARRY samples using a Leica M205C binocular microscope using transmitted and polarized light. E. Morley picked CD samples at the University of Calgary. Selected grains were screened for quality to ensure they were free from inclusions or other crystal defects and were of sufficient size. Between 12 and 3 individual grains were selected from each sample. Each grain was measured and photographed before being packed. HG and BARRY apatite and zircon samples were sent to CU-TRaIL at the University of Colorado, Boulder for (U-Th)/He analysis. At CU-TRaIL each grain was heated with a 25W diode laser to allow for the diffusion of Helium through the crystal lattice. This procedure was repeated at least once to ensure the grain was completely degassed and determine the presence of inclusions. Helium concentration was measured on a mass spectrometer attached to the laser stage. After degassing, samples were dissolved in acid. Apatite was dissolved in HNO^3 at 80^{o}C and zircon with a multi-step acid-vapor dissolution using HF, HCl, and HNO^3. Dissolved grains were spiked and analyzed for U, Th, and Sm content on an ICP-MS. From these data, cooling ages were calculated using the protocol of Ketcham (2011). CD samples were processed at the University of Calgary using the protocol of the CPATT lab.

Apatite Fission Track Thermochronometry

All apatite fission track analyses were done by Blythe. Apatites were mounted in epoxy. Sample surfaces were ground and polished. Apatite mounts were etched in 5.5M HNO3 at 18°C for 22s. An “external detector” (e.g., Naeser, 1979), consisting of low-U <5 ppb) Brazil Ruby muscovite, was used for each sample. Samples were irradiated in the Oregon State Triga nuclear reactor. Following irradiation, the muscovites were etched in 48% HF at 18°C for 30 min. Tracks were counted using a 100X dry lens and 1250X total magnification in crystals with well-etched, clearly visible tracks and sharp polishing scratches. A Kinitek stage and software written by Dumitru (1993) were used for analyses. Parentheses show number of tracks counted. Standard and induced track densities were determined on external detectors (geometry factor = 0.5), and fossil track densities were determined on internal mineral surfaces. Ages were calculated using

zeta 359 ± 10 (AB) for dosimeter CN-5 (e.g., Hurford and Green, 1983). All ages are central ages, with the conventional method (Green, 1981) used to determine errors on sample ages. The chi-square test estimated the probability that individual grain ages for each sample belong to a single population with Poissonian distribution (Galbraith, 1981). The data were reduced with the program Binomfit (Brandon, 2002).

2. Sample Locations and Data

Sample	Lithology	Longitude (E)	Latitude (N)	Elevation (m)	#Ahe	#Zhe	#AFT
06CD16	Honna Sandstone	-132.118	53.204	0	9	0	0
07CD16	Yakoun Sandstone	-132.080	53.215	0	10	0	0
21CD16	Longarm Sandstone	-132.319	53.226	0	2	0	0
29CD16	Honna Sandstone	-132.149	53.230	0	12	0	0
BARRY	San Christoval Amphibolite	-131.753	52.576	794	4	3	16
HG02	Burnaby Island Diorite	-131.562	52.595	0	5	0	20
HG03	Burnaby Island Diorite	-131.586	52.581	0	5	0	0
HG04	San Christoval Diorite	-131.569	52.551	0	5	3	20
HG05	San Christoval Diorite	-131.691	52.528	347	5	0	0
HG06	San Christoval Diorite	-131.678	52.533	0	5	0	0
HG09	Kano Diorite	-131.146	52.307	0	5	0	0
HG10	San Christoval Diorite	-131.146	52.188	0	5	0	0
HG12	San Christoval Diorite	-131.097	52.006	0	5	3	20
HG15	San Christoval Diorite	-132.047	52.746	914	5	0	0
HG17	Kano Diorite	-131.927	52.989	0	3	0	0
HG19	Honna Conglomerate	-131.816	53.037	0	4	0	0
HG28	San Christoval Diorite	-132.511	53.352	0	5	3	30
HG29	Burnaby Island Diorite	-132.480	53.363	0	4	0	0
HG32	San Christoval Diorite	-131.889	52.655	0	4	0	0
HG34	Kano Diorite	-131.768	52.530	0	5	0	20

Apatite (U-Th)/He data from Haida Gwaii

Sample	Grain	Mass (μg)	r[a] (μm)	T[b]	He (nmol/g)	U (ppm)	Th (ppm)	Sm (ppm)	eU[c] (ppm)	Th/U	Raw Date (Ma)	Ft[d]	Date (Ma)	2σ[e] (Ma)
BARRY														
Amphibolite of San Christoval Plutonic Suite, Emplacement 170 ±10 Ma														
	a	1.02	39.01	2	7.15	145.53	167.16	15.47	184.8	1.15	7.16	0.64	11.16	0.24
	b[f]	*0.65*	*33.25*	*2*	*4.79*	*111.71*	*137.08*	*12.58*	*143.9*	*1.23*	*6.16*	0.58	*10.61*	*0.31*
	c	0.76	35.65	2	5.02	114.44	132.68	11.81	145.6	1.16	6.38	0.61	10.45	0.44
	d	1.42	43.32	2	5.53	114.55	142.88	18.85	148.1	1.25	6.90	0.68	10.20	0.28
Mean: 10.6 ± 0.5 Ma														
HG02														
Diorite of Burnaby Island Plutonic Suite, Emplacement 160 ±10 Ma														
	a	1.87	46.77	2	0.36	20.75	31.61	11.53	28.2	1.52	2.38	0.69	3.43	0.22
	b	0.83	34.21	2	0.26	11.32	5.84	9.80	12.7	0.52	3.83	0.60	6.40	0.78
	c	2.53	45.77	1	0.40	11.75	13.51	7.36	14.9	1.15	4.97	0.69	7.21	0.37
	d	1.76	44.00	1	0.59	19.02	15.14	9.82	22.6	0.80	4.82	0.68	7.04	0.40
	e	2.25	45.12	1	0.44	20.91	29.42	10.31	27.8	1.41	2.91	0.68	4.25	0.26
Mean: 5.7 ± 1.7 Ma														
HG03														
Diorite of Burnaby Island Plutonic Suite, Emplacement 160 ±10 Ma														
	a	3.43	50.90	2	1.21	41.80	21.45	11.52	46.8	0.51	4.80	0.72	6.63	0.27
	b	3.60	53.92	1	1.35	40.21	25.20	7.10	46.1	0.63	5.40	0.74	7.30	0.28
	c	1.36	43.28	2	1.75	51.72	25.42	8.49	57.7	0.49	5.63	0.68	8.26	0.25
	d	1.91	45.94	2	1.59	46.50	27.18	9.99	52.9	0.59	5.58	0.70	8.02	0.40
	e	1.07	36.67	2	1.68	54.67	27.97	12.88	61.2	0.51	5.08	0.62	8.16	0.45
Mean: 7.7 ± 0.7 Ma														
HG04														
Diorite of San Christoval Plutonic Suite, Emplacement 170 ±10 Ma														
	a	1.04	39.51	2	2.45	63.06	69.47	18.33	79.4	1.10	5.70	0.65	8.82	0.50
	b	2.05	44.13	2	2.37	47.71	67.10	15.82	63.5	1.41	6.88	0.68	10.17	0.27
	c	1.52	44.11	2	2.03	47.89	54.91	14.64	60.8	1.15	6.16	0.68	9.05	0.31
	d	1.91	44.99	1	1.52	42.85	51.72	12.09	55.0	1.21	5.11	0.69	7.42	0.31
	e	1.47	40.71	2	1.72	43.84	50.61	15.07	55.7	1.15	5.69	0.65	8.72	0.46
Mean: 8.8 ± 1.0 Ma														
HG05														
Diorite of San Christoval Plutonic Suite, Emplacement 170 ±10 Ma														
	a[g]	*2.76*	*53.93*	*2*	*2.45*	*44.17*	*69.49*	*11.46*	*60.5*	*1.57*	*5.99*	*0.73*	*8.17*	*0.31*
	b	1.02	39.36	2	2.37	66.20	108.56	16.74	91.7	1.64	5.64	0.64	8.80	0.49
	c	1.12	38.02	2	2.03	93.94	147.25	20.95	128.5	1.57	5.33	0.62	8.53	0.30
	d[g]	*1.17*	*40.73*	*2*	*1.52*	*77.67*	*123.13*	*15.87*	*106.6*	*1.59*	*4.29*	*0.65*	*6.57*	*0.22*
	e	1.26	41.90	2	1.72	57.15	87.89	14.47	77.8	1.54	5.32	0.66	8.03	0.32

Mean: 8.5 ± 0.4 Ma

HG06

Diorite of San Christoval Plutonic Suite, Emplacement 170 ±10 Ma

a	1.11	37.83	1	4.62	130.99	164.37	14.03	169.6	1.26	5.04	0.63	7.95	0.29
b	1.00	37.71	2	5.79	157.15	166.69	15.37	196.3	1.06	5.46	0.63	8.66	0.37
c	1.45	44.56	2	5.59	188.94	236.24	12.57	244.5	1.25	4.23	0.68	6.18	0.18
d	3.48	57.25	2	2.15	76.31	95.48	7.61	98.7	1.25	4.02	0.75	5.37	0.16
e	1.74	45.73	2	3.60	118.61	132.09	14.98	149.7	1.11	4.45	0.69	6.44	0.22

Mean: 6.9 ± 1.3 Ma

HG09

Diorite of Kano Plutonic Suite, Emplacement 40 ±10 Ma

a	2.47	47.94	1	0.59	6.39	13.52	35.77	9.6	2.11	11.07	0.70	15.69	0.94
b [h]	*1.62*	*42.52*	*1*	*6.99*	*11.35*	*63.06*	*35.95*	*26.2*	*5.56*	*48.63*	*0.65*	*74.21*	*2.66*
c	1.16	37.55	1	0.70	6.39	9.95	51.83	8.7	1.56	14.10	0.63	22.09	1.77
d [f]	*0.74*	*33.30*	*1*	*6.21*	*10.84*	*30.42*	*58.87*	*18.0*	*2.81*	*61.91*	*0.58*	*104.99*	*9.45*
e	0.98	38.07	2	0.85	7.33	10.26	56.03	9.7	1.40	15.33	0.63	23.92	3.54

Mean: 20.6 ± 4.3 Ma

HG10

Diorite of San Christoval Plutonic Suite, Emplacement 170 ±10 Ma

a	1.28	41.69	2	2.23	68.72	33.26	12.93	76.5	0.48	5.40	0.67	8.08	0.28
b	2.90	51.34	1	1.41	49.05	30.07	9.57	56.1	0.61	4.65	0.73	6.39	0.25
c	0.87	36.51	2	2.06	80.74	41.57	12.99	90.5	0.51	4.22	0.62	6.78	0.36
d	0.77	35.64	2	2.61	92.17	52.16	15.86	104.4	0.57	4.62	0.62	7.50	0.49
e	2.05	46.72	1	1.34	48.21	29.50	10.44	55.1	0.61	4.49	0.70	6.37	0.16

Mean: 7 ± 0.7 Ma

HG12

Diorite of San Christoval Plutonic Suite, Emplacement 170 ±10 Ma

a	2.69	49.46	2	0.87	21.47	21.34	19.73	26.5	0.99	6.02	0.71	8.44	0.45
b	1.98	45.58	2	1.34	28.00	30.43	29.12	35.1	1.09	7.04	0.69	10.20	0.30
c	1.72	44.50	2	1.27	24.87	28.09	30.48	31.5	1.13	7.40	0.68	10.83	0.87
d	3.65	52.73	1	0.80	15.37	19.76	18.30	20.0	1.29	7.32	0.73	10.02	0.42
e	3.19	51.48	1	1.10	21.99	28.28	21.78	28.6	1.29	7.07	0.72	9.76	0.45

Mean: 9.9 ± 0.9 Ma

HG15

Diorite of San Christoval Plutonic Suite, Emplacement 170 ±10 Ma

a [g]	*3.81*	*50.83*	*0*	*0.53*	*7.53*	*12.15*	*28.57*	*10.4*	*1.61*	*9.21*	*0.72*	*12.71*	*0.75*
b	2.82	49.01	1	0.50	12.75	20.46	37.19	17.6	1.61	5.21	0.71	7.33	0.29
c [g]	*6.31*	*63.73*	*0*	*0.83*	*13.95*	*17.98*	*24.79*	*18.2*	*1.29*	*8.40*	*0.78*	*10.79*	*0.41*
d [g]	*8.49*	*68.81*	*0*	*0.60*	*7.09*	*12.24*	*21.60*	*10.0*	*1.73*	*10.98*	*0.79*	*13.86*	*0.50*
e	2.28	45.67	1	0.59	15.09	18.97	46.57	19.6	1.26	5.47	0.69	7.88	0.45

Mean: 7.6 ± 0.4 Ma

HG17

Diorite of Kano Plutonic Suite, Emplacement 30 ±10 Ma

a[f]	*1.15*	*37.13*	*0*	*3.32*	*25.55*	*45.01*	*68.18*	*36.1*	*1.76*	*16.74*	*0.63*	*26.52*	*1.20*
b[f]	*2.35*	*44.37*	*0*	*0.84*	*6.70*	*7.29*	*40.09*	*8.4*	*1.09*	*17.75*	*0.68*	*25.65*	*2.52*
c[f]	*1.57*	*39.98*	*0*	*2.33*	*19.49*	*32.37*	*68.52*	*27.1*	*1.66*	*15.58*	*0.65*	*23.82*	*1.38*

Mean: --

HG19

Conglomerate of Honna Formation, Deposition 90 ±10 Ma

a	3.14	57.36	2	2.88	25.35	36.90	42.09	34.0	1.46	15.52	0.75	20.61	0.77
b	2.90	52.62	2	0.74	9.94	16.50	16.18	13.8	1.66	9.81	0.72	13.50	0.70
c	3.32	54.75	1	1.06	12.31	24.22	11.13	18.0	1.97	10.85	0.74	14.70	0.71
d	1.20	41.27	2	2.02	23.51	29.28	45.10	30.4	1.25	12.17	0.66	18.38	1.88

Mean: 16.8 ± 3.3 Ma

HG28

Diorite of San Christoval Plutonic Suite, Emplacement 170 ±10 Ma

a	3.95	56.20	1	0.70	21.13	14.43	19.71	24.5	0.68	5.22	0.75	6.96	0.26
b[f]	*1.23*	*40.33*	*2*	*0.19*	*6.28*	*8.12*	*26.81*	*8.2*	*1.29*	*4.29*	*0.65*	*6.55*	*1.14*
c	2.10	50.03	2	0.23	7.64	9.33	26.58	9.8	1.22	4.32	0.72	5.99	0.69
d	3.13	56.57	2	0.20	5.34	6.92	26.02	7.0	1.30	5.25	0.75	6.98	0.52
e	1.24	41.70	2	0.27	11.10	12.55	27.30	14.1	1.13	3.51	0.66	5.26	0.38

Mean: 6.3 ± 0.8 Ma

HG29

Diorite of Burnaby Island Plutonic Suite, Emplacement 160 ±10 Ma

a	1.22	40.07	2	0.22	10.44	8.05	34.83	12.3	0.77	3.24	0.65	4.93	0.67
b	1.51	43.17	2	0.44	10.57	13.77	40.40	13.8	1.30	5.71	0.67	8.44	0.68
c	1.39	41.26	2	0.36	12.55	12.31	43.94	15.4	0.98	4.17	0.66	6.28	0.63
d	2.30	47.35	1	0.24	6.29	7.40	30.77	8.0	1.18	5.34	0.70	7.54	0.70

Mean: 6.8 ± 1.5 Ma

HG32

Diorite of Burnaby Island Plutonic Suite, Emplacement 160 ±10 Ma

a	1.89	46.21	2	0.94	15.35	38.84	8.77	24.5	2.53	7.08	0.68	10.32	0.61
b[f]	*1.90*	*45.62*	*2*	*0.94*	*24.99*	*42.38*	*13.85*	*35.0*	*1.70*	*4.95*	*0.68*	*7.23*	*0.33*
c	1.60	44.26	2	1.19	19.49	36.36	9.39	28.0	1.86	7.82	0.67	11.56	0.31
d[f]	*1.59*	*45.44*	*2*	*1.28*	*31.16*	*62.88*	*10.79*	*45.9*	*2.02*	*5.15*	*0.68*	*7.52*	*0.26*

Mean: 10.9 ± 0.9 Ma

HG34

Diorite of Kano Plutonic Suite, Emplacement 40 ±10 Ma

a	1.25	41.11	2	1.57	46.83	32.92	30.66	54.6	0.70	5.31	0.66	8.02	0.41
b	2.69	51.52	1	1.31	47.05	13.91	13.24	50.3	0.30	4.82	0.73	6.57	0.43
c[f]	*2.22*	*48.15*	*1*	*1.36*	*42.48*	*18.73*	*16.71*	*46.9*	*0.44*	*5.36*	*0.71*	*7.49*	*0.36*

d	1.14	40.20	2	1.25	49.00	25.22	21.39	54.9	0.51	4.22	0.66	6.42	0.41
e[f]	*1.20*	*39.88*	*2*	*1.08*	*35.59*	*25.15*	*16.78*	*41.5*	*0.71*	*4.80*	*0.65*	*7.38*	*0.63*

Mean: 7 ± 0.9 Ma

06CD16

Sandstone of Honna Formation, Deposition 90 ±5 Ma

a	6.23	58.30	2	0.43	3.53	11.63	-	6.3	3.41	12.63	0.76	16.61	1.07
b	2.41	42.50	2	0.46	5.87	11.35	-	8.5	2.00	10.08	0.68	14.83	0.95
c	1.31	34.80	2	1.55	19.95	44.34	-	30.4	2.30	9.51	0.62	15.41	0.82
d	1.38	36.00	2	0.36	4.26	14.77	-	7.7	3.59	8.60	0.63	13.67	1.12
e	1.18	33.70	2	0.46	8.64	18.88	-	13.1	2.26	6.60	0.61	10.89	0.82
f	4.31	53.40	2	0.49	5.44	12.01	-	8.3	2.28	10.98	0.74	14.84	0.95
g	2.65	44.00	2	0.48	8.50	11.00	-	11.9	1.34	7.97	0.69	11.56	0.74
h	2.77	44.30	2	0.81	13.79	20.38	-	18.6	1.53	8.08	0.69	11.69	0.69
i	3.23	45.00	2	0.31	5.75	9.98	-	8.1	1.79	7.18	0.70	10.33	0.69

Mean: 13.31 ± 2.25 Ma

07CD16

Sandstone of Yakoun Formation, Deposition 170 ±3 Ma

a	2.17	36.10	2	0.07	0.78	2.87	-	1.5	3.79	9.50	0.63	15.80	3.03
b	5.96	53.80	2	0.12	0.82	2.66	-	1.5	3.39	15.19	0.74	20.50	1.67
c	2.03	39.30	2	0.08	0.77	2.30	-	1.3	3.09	11.31	0.65	17.30	3.61
d	4.68	51.70	2	0.10	0.83	2.29	-	1.4	2.86	13.20	0.73	18.06	1.82
e[h]	*3.13*	*47.60*	*2*	*0.10*	*0.53*	*1.79*	-	*1.0*	*3.49*	*20.39*	*0.71*	*28.63*	*3.54*
f	3.23	45.00	2	0.09	0.65	1.74	-	1.1	2.75	15.29	0.70	22.00	3.02
g	2.84	42.70	2	0.09	0.83	2.72	-	1.5	3.39	10.98	0.68	16.14	2.40
h	7.59	61.90	2	0.09	0.72	1.79	-	1.1	2.57	15.05	0.77	19.47	1.65
i	2.34	41.10	2	0.12	0.72	2.33	-	1.3	3.35	16.96	0.67	25.36	3.43
j	22.96	88.70	2	0.12	0.73	2.01	-	1.2	2.84	19.24	0.84	22.96	1.63

Mean: 19.73 ± 3.26 Ma

21CD16

Sandstone of Longarm Formation, Deposition 112 ±5 Ma

a	1.47	37.00	2	0.50	10.24	23.42	-	15.7	2.36	5.95	0.64	9.33	0.64
b	0.97	31.40	2	0.66	25.63	22.47	-	30.9	0.91	3.99	0.58	6.88	0.46

Mean: 8.11 ± 1.73 Ma

29CD16

Sandstone of Honna Formation, Deposition 90 ±5 Ma

a[h]	*2.17*	*42.30*	*2*	*0.49*	*2.19*	*5.92*	-	*3.6*	*2.79*	*25.36*	*0.68*	*37.40*	*2.44*
b[h]	*1.45*	*35.50*	*2*	*0.98*	*3.65*	*14.19*	-	*6.9*	*4.12*	*26.23*	*0.62*	*42.03*	*2.38*
c	1.14	33.50	2	2.27	35.16	45.88	-	45.9	1.35	9.18	0.61	15.15	0.79
d	*1.65*	*37.90*	*2*	*0.85*	*4.76*	*17.02*	-	*8.8*	*3.70*	*17.99*	*0.65*	*27.89*	*1.64*
e	1.72	36.70	2	0.25	3.21	11.25	-	5.9	3.62	7.96	0.63	12.56	1.13
f	*2.31*	*39.10*	*2*	*0.53*	*3.59*	*18.44*	-	*7.9*	*5.31*	*12.35*	*0.65*	*18.91*	*1.16*
g	1.58	38.10	2	0.19	2.82	8.26	-	4.8	3.03	7.50	0.65	11.59	1.38

h [h]	*7.50*	*62.90*	*2*	*0.29*	*14.67*	*30.84*	-	*21.9*	*2.17*	*2.46*	*0.78*	*3.17*	*0.21*
i	1.69	36.50	2	0.22	1.77	8.57	-	3.8	5.00	10.97	0.63	17.36	1.71
j	2.01	39.90	2	0.30	3.12	8.17	-	5.0	2.71	10.99	0.66	16.63	1.30
k [h]	*6.51*	*61.70*	*2*	*0.98*	*7.24*	*17.60*	-	*11.4*	*2.51*	*15.98*	*0.77*	*20.65*	*1.34*
l	5.29	53.20	2	0.47	3.99	14.09	-	7.3	3.65	12.05	0.74	16.33	1.03

Mean: 14.94 ± 2.35 Ma

---

[a] equivelent spherical radius

[b] F T indicates grain terminus. 0: Both tips broken. 1:One tip broken. 2: Whole grain.

[c] eU - effective uranium concentration, weights U and Th for their alpha productivity, computed as [U] + 0.235 * [Th]

[d] Ft is alpha-ejection correction of Farley et al [2002]

[e] Analytical uncertainty based on U, Th, He, and grain length measurements

Grains in grey were not included in means, plots or models and were excluded for the following reasons:

[f] Grains with Ft <0.6

[g] Apatite grains with He re-extraction < 98%

[h] Grains that failed the Peirce outlier test (Ross, 2003)

Apatite Fission Track data from Haida Gwaii

Sample	# grains	Standard track density x10^6 cm^{-2} (# counted)	Fossil track density x 10^5 cm^{-2} (# counted)	Induced track density x10^6 cm^{-2} (# counted)	Chi square prob. %	Dpar in um	Central age (Ma) (95% CI)	Mean length in um (# measured)
BARRY	16	1.44 (2315)	3.34 (66)	6.82 (1348)	99	-	12.9 (+3.7/-2.9)	13.53 ± 1.1 (9)
HG02	20	1.53 (2465)	0.43 (24)	1.17 (660)	95	-	10.0 (+5.1/-3.4)	-
HG04	20	1.5 (2425)	1.41 (77)	3.38 (1854)	97	2.30	11.2 (+3.0/-2.4)	14.9 ± 0.9 (4)
HG12	20	1.5 (2415)	1.35 (84)	2.7 (1683)	95	2.60	13.4 (+3.4/-2.7)	15.0 ± 0.8 (4)
HG28	30	1.47 (2365)	0.21 (19)	0.44 (409)	92	-	12.2 (+7.2/-4.5)	13.1 ± 1.5 (4)
HG34	20	1.47 (2365)	1.67 (56)	4.18 (1405)	99	2.20	10.5 (+3.3/-2.5)	14.7 ± 1.0 (5)

Zircon (U-Th)/He data from Haida Gwaii

Sample	Grain	Mass (µg)	r[a] (µm)	T[b]	He (nmol/g)	U (ppm)	Th (ppm)	Sm (ppm)	eU[c] (ppm)	Th/U	Raw Date (Ma)	Ft[d]	Date (Ma)	2σ[e] (Ma)
HG04														
Diorite of San Christoval Plutonic Suite, Emplacement 170 ±10 Ma														
	a	5.7	57.0	2	15.83	119.8	37.6	0.1	128.6	1.149	7.16	0.801	28.44	0.66
	b[f]	*5.5*	*56.1*	*2*	*31.8*	*447.2*	*75.1*	*0.7*	*464.8*	*1.227*	*6.16*	*0.799*	*15.88*	*0.94*
	c	6.0	56.3	2	19.2	160.6	55.4	0.1	173.6	1.159	6.38	0.798	25.60	0.81
Mean: 27 ± 2 Ma														
HG12														
Diorite of San Christoval Plutonic Suite, Emplacement 170 ±10 Ma														
	a	5.21	53.93	2	25.751	182.13	62.88	0.46	196.9	0.345	24.21	0.790	30.63	0.84
	b	3.85	48.18	2	20.975	141.30	48.09	0.04	152.6	0.340	25.45	0.766	33.19	1.49
	c	5.75	57.34	2	18.975	114.90	37.39	0.15	123.7	0.325	28.40	0.802	35.38	0.85
Mean: 33.1 ± 2.4 Ma														
HG28														
Diorite of San Christoval Plutonic Suite, Emplacement 170 ±10 Ma														
	a	5.98	54.75	2	19.396	60.63	26.61	0.42	66.9	0.439	53.55	0.792	67.52	4.45
	b	11.75	70.69	2	18.706	66.85	24.48	0.45	72.6	0.366	47.60	0.838	56.77	2.79
	c	4.16	52.07	2	18.445	75.33	28.86	0.54	82.1	0.383	41.53	0.783	52.99	1.78
Mean: 59.1 ± 7.5 Ma														

[a] equivelent spherical radius

[b] F T indicates grain terminus. 0: Both tips broken. 1:One tip broken. 2: Whole grain.

[c] eU - effective uranium concentration, weights U and Th for their alpha productivity, computed as [U] + 0.235 * [Th]

[d] Ft is alpha-ejection correction of Farley et al [2002]

[e] Analytical uncertainty based on U, Th, He, and grain length measurements

Grains in grey were not included in means, plots or models and were excluded for the following reasons:

[f] Outlier

3. Description of thermal model parameters

QTQt v. 5.7.0 modeling

We model 11 of 20 samples using the QTQt software package (Gallagher, 2012). QTQt uses a Bayesian transdimensional Markov Chain Monte Carlo method to invert thermochronometry data for time-temperature histories. Samples were selected for modeling if they had multiple thermochronometers, were collected from sedimentary rocks, or made up part of a vertical transect.

For 6 samples, we ran the model for 100,000 burn-in and 500,000 post burn-in steps. For samples with AHe, ZHe, and AFT thermochronometers, we ran models for 500,000 burn-in and 1,000,000 post burn-in steps. Proposals outside the prior were rejected and inversions rejected more complex models that did not improve data fit. For sedimentary and igneous samples, we did not add a deposition/crystallization age constraint as we found this constraint over determines model outcomes. All samples use the RDAAM diffusion model for apatite (Flowers et al., 2009), ZRDAAM for zircon (Guenthener et al., 2013), and the fission track annealing model outlined by Ketcham et al., (2007). Errors on all Helium dates were re-sampled to address uncertainty not accounted for in recorded analytical error (Gallagher, 2012).

Interpretation of model results was based on the expected model, which is a mean model weighted by each model's posterior probability and the 95% credible interval around the expected model (Gallagher, 2012). Below, we provide QTQt input information for each sample as well as model results.

4. QTQt model input data

A. Barry Inlet vertical transect

Table S1.1 Data inputs for Barry Inlet vertical transect.

Sample #	Elev. (m)	Unit + Emplacement Age (Ma)	Systems used
HG04	0	San Christoval Plutonic Suite* 170±10	AHe, AFT, ZHe
HG05	347	San Christoval Plutonic Suite* 170±10	AHe
BARRY	794	San Christoval Plutonic Suite* 170±10	AHe, AFT

*Lewis et al., 1991

Table S1.2 Thermal history constraints for model for Barry Inlet vertical transect

Range for Time (Myr) general prior	Range for Temp (˚C) general prior	Geologic unit and depositional or emplacement age	Temperature gradient (˚C/km)	Present Day Surface Temp (˚C)	Present Day temperature gradient (˚C/km)	Max. ∂T/∂t (˚C/Myr)
22.79 ± 22.79*	100 ± 100	--	30 ± 30	5 ± 5	2.5±2.5	1000

*oldest single grain age

Table S1.3 Apatite and zircon-helium inputs Barry Inlet vertical transect.

Raw Date (Ma)	Error	eU (ppm)	Grain length (microns)	Grain width (microns)	Grain thickness (microns)
Sample HG04 (apatite)					
5.7	0.16	79.4	119	85.8	79.4
6.88	0.09	63.5	193	70.5	63.5
6.16	0.1	60.8	142	83.3	87.3
5.11	0.1	55	138	84.7	87.6
5.69	0.15	55.7	165	84.3	69.4
Sample HG04 (zircon)					
22.79	0.26	128.6	193	103	93
20.45	0.32	173.6	209.5	103	85
Sample HG05					
5.64	0.16	91.7	147	65.8	69.4
5.33	0.09	128.5	147	65.8	69.4
5.32	0.1	77.8	128	85.8	83.2
Sample BARRY					
7.16	0.07	184.8	120	81	73

6.38	0.13	145.6	105	79	66
6.9	0.1	148.1	121	122	81

Table S1.4 Apatite fission track data for Barry Inlet vertical transect

Sample HG04			
Zeta	**Dpar**	**Nd**	
359±10	2.3	2425	
Ns	**Ni**	**Date (Ma)**	**Date error**
4	120	8.97	4.562
5	123	10.94	4.994
1	99	2.72	2.733
3	78	10.35	6.092
4	90	11.96	6.114
6	109	14.8	6.215
4	118	9.12	4.641
6	106	15.22	6.396
6	143	11.29	4.709
5	81	16.6	7.656
1	89	3.02	3.042
5	87	15.46	7.115
3	51	15.82	9.403
5	104	12.93	5.926
2	80	6.73	4.818
5	96	14.01	6.432
6	112	14.41	6.045
2	71	7.58	5.437
1	36	7.47	7.579
3	61	13.23	7.827
Sample BARRY			
Zeta	**Dpar**	**Nd**	
359±10	2.3	2315	
Ns	**Ni**	**Date (Ma)**	**Date error**
3	91	8.52	5
5	81	15.94	7.351

1	34	7.6	7.71
6	117	13.24	5.55
5	90	14.34	6.597
6	141	10.99	4.587
5	64	20.16	9.372
7	123	14.69	5.718
3	79	9.81	5.773
1	44	5.87	5.939
4	94	10.99	5.615
3	66	11.74	6.934
6	107	14.48	6.081
3	51	15.19	9.028
4	102	10.13	5.167
4	64	16.13	8.322

B. Sample HG02

Table S2.1 Data inputs for HG02

Sample #	Elev. (m)	Unit + Emplacement Age (Ma)	Systems used
HG02	0	Burnaby Island Plutonic Suite* 160±10	AHe, AFT

*Lewis et al., 1991

Table S2.2 Thermal history constraints for model for HG02

Range for Time (Myr) general prior	Range for Temp (˚C) general prior	Geologic unit and depositional or emplacement age	Present Day Surface Temp (˚C)	Max. ∂T/∂t (˚C/ Myr)
9.98 ± 9.98*	70 ± 70	--	10 ± 0	1000

*oldest single grain age

Table S2.3 Apatite and zircon-helium inputs HG02

Raw Age (Ma)	Error	eU (ppm)	Grain length (microns)	Grain width (microns)	Grain thickness (microns)
Sample HG02 (apatite)					
2.38	0.07	28.2	159	93	79
2.91	0.09	27.8	178	85.1	70.5
4.97	0.12	14.9	199	87.7	66
4.82	0.13	22.6	132	90.9	74.8
3.83	0.24	27.8	132	72.5	59

Note: Bimodal AHe age distribution – models run for both old and young AHe age groups.

Table S2.4 Apatite fission track data for HG02

Sample HG02			
Zeta	**Dpar**	**Nd**	
359±10	2.2	2465	
Ns	**Ni**	**Date (Ma)**	**Date error**
0	10	0	95.219
1	53	5.18	5.229
2	28	19.59	14.342
2	58	9.46	6.809
2	41	13.38	9.695

1	19	14.44	14.816
0	29	0	29.818
2	54	10.16	7.322
2	43	12.76	9.234
0	49	0	17.291
2	45	12.19	8.816
1	20	13.72	14.059
1	30	9.15	9.301
2	30	18.28	13.357
0	24	0	36.409
1	20	13.72	14.059
1	5	54.69	59.925
2	44	12.47	9.02
1	24	11.43	11.671
1	34	8.07	8.19

C. Sample HG12

Table S3.1 Data inputs for HG12

Sample #	Elev. (m)	Unit + Emplacement Age (Ma)	Systems used
HG12	0	San Christoval Plutonic Suite* 170±10	AHe, AFT, ZHe

*Lewis et al., 1991

Table S3.2 Thermal history constraints for model for HG12

Range for Time (Myr) general prior	Range for Temp (˚C) general prior	Geologic unit and depositional or emplacement age	Present Day Surface Temp (˚C)	Max. ∂T/∂t (˚C/ Myr)
28.4 ± 28.4*	100 ± 100	--	10 ± 0	1000

*oldest single grain age

Table S3.3 Apatite and zircon-helium inputs HG12

Raw Date (Ma)	Error	eU (ppm)	Grain length (microns)	Grain width (microns)	Grain thickness (microns)
Sample HG12 (apatite)					
6.02	0.16	26.5	211	91.7	75.6
7.04	0.1	25.1	176	103	77
7.4	0.3	31.5	160	95	79
7.32	0.15	20	213	94.8	89.7
7.07	0.16	28.6	185	99.7	92.7
Sample HG12 (zircon)					
24.21	0.33	196.9	199.5	100	81
25.45	0.57	152.6	182.5	95	69
28.4	0.34	123.7	192.5	103	95

Table S3.4 Apatite fission track data for HG12

Sample HG12			
Zeta	**Dpar**	**Nd**	
359±10	2.6	2415	
Ns	**Ni**	**Date (Ma)**	**Date error**
2	53	10.15	7.316
6	95	16.98	7.157

5	114	11.8	5.396
5	147	9.15	4.166
7	137	13.74	5.333
2	52	10.35	7.459
7	114	16.51	6.438
3	96	8.41	4.933
3	50	16.13	9.596
2	70	7.69	5.516
4	56	19.2	9.946
1	27	9.96	10.149
0	45	0	18.508
3	47	17.16	10.227
3	35	23.04	13.867
4	41	26.21	13.742
9	203	11.93	4.07
4	77	13.97	7.171
2	47	11.45	8.268
12	177	18.23	5.45

D. Sample HG19

Table S4.1 Data inputs for HG19

Sample #	Elev. (m)	Unit + Deposition Age (Ma)	Systems used
HG19	0	Honna Formation* 95±5	AHe

*Lewis et al., 1991

Table S4.2 Thermal history constraints for model for HG19

Range for Time (Myr) general prior	Range for Temp (˚C) general prior	Geologic unit and depositional or emplacement age	Present Day Surface Temp (˚C)	Max. ∂T/∂t (˚C/ Myr)
15.52 ± 15.52*	70 ± 70	--	10 ± 0	1000

*oldest single grain age

Table S4.3 Apatite and zircon-helium inputs HG19

Raw Date (Ma)	Error	eU (ppm)	Grain length (microns)	Grain width (microns)	Grain thickness (microns)
Sample HG19 (apatite)					
15.52	0.29	34	165	119	126
9.81	0.25	13.8	198	102	82.7
10.85	0.26	18	157	113	98.9
12.17	0.61	30.4	126	86.9	76.3

E. Sample HG28

Table S5.1 Data inputs for HG28

Sample #	Elev. (m)	Unit + Emplacement Age (Ma)	Systems used
HG28	0	San Christoval Plutonic Suite* 170±10	AHe, AFT, ZHe

*Lewis et al., 1991

Table S5.2 Thermal history constraints for model for HG28

Range for Time (Myr) general prior	Range for Temp (˚C) general prior	Geologic unit and depositional or emplacement age	Present Day Surface Temp (˚C)	Max. ∂T/∂t (˚C/Myr)
53.55 ± 53.55*	100 ± 100	--	10 ± 0	1000

*oldest single grain age

Table S5.3 Apatite and zircon-helium inputs HG28

Raw Date (Ma)	Error	eU (ppm)	Grain length (microns)	Grain width (microns)	Grain thickness (microns)
Sample HG28 (apatite)					
5.22	0.09	24.5	192	110	92
4.32	0.25	9.8	148	110	92.7
5.25	0.19	7	175	126	93.8
3.51	0.12	14.1	127	93.8	70.3
Sample HG28 (zircon)					
53.55	1.78	66.9	217.5	113	75
47.6	1.17	72.6	264.5	122	111
41.53	0.7	82.1	164.5	103	86

Table S5.4 Apatite fission track data for HG28

Sample HG28			
Zeta	**Dpar**	**Nd**	
359±10	2.3	2365	
Ns	**Ni**	**Date (Ma)**	**Date error**
0	14	0	62.652
0	16	0	54.104
2	29	18.17	13.29

0	8	0	118.751
1	17	15.5	15.955
0	13	0	68.022
1	9	29.25	30.84
0	8	0	118.751
3	30	26.33	15.954
0	13	0	68.022
0	10	0	91.511
0	7	0	139.419
1	20	13.18	13.508
1	8	32.9	34.901
1	12	21.95	22.852
0	11	0	82.074
3	23	34.33	21.083
0	8	0	118.751
1	19	13.87	14.236
0	16	0	54.104
1	11	23.94	25.013
2	15	35.09	26.422
0	11	0	82.074
0	12	0	74.393
0	7	0	139.419
0	21	0	40.332
0	10	0	91.511
1	12	21.95	22.852
1	16	17.57	18.147
0	4	0	287.628

F. Sample HG34

Table S6.1 Data inputs for HG34

Sample #	Elev. (m)	Unit + Emplacement Age (Ma)	Systems used
HG34	0	Kano Plutonic Suite* 40±10	AHe, AFT

*Lewis et al., 1991

Table S6.2 Thermal history constraints for model for HG34

Range for Time (Myr) general prior	Range for Temp (˚C) general prior	Geologic unit and depositional or emplacement age	Present Day Surface Temp (˚C)	Max. ∂T/∂t (˚C/Myr)
10.51 ± 10.51*	70 ± 70	--	10 ± 0	1000

*oldest single grain age

Table S6.3 Apatite and zircon-helium inputs HG34

Raw Date (Ma)	Error	eU (ppm)	Grain length (microns)	Grain width (microns)	Grain thickness (microns)
Sample HG34 (apatite)					
5.31	0.13	54.6	137	82.7	70
4.82	0.15	50.3	136	109	102
4.8	0.2	41.5	142	77	67

Table S6.4 Apatite fission track data for HG34

Sample HG34			
Zeta	**Dpar**	**Nd**	
359±10	2.2	2365	
Ns	**Ni**	**Date (Ma)**	**Date error**
2	55	9.59	6.905
8	171	12.33	4.468
1	22	11.98	12.255
2	42	12.55	9.089
5	80	16.47	7.6
2	85	6.21	4.441
2	61	8.65	6.215
4	80	13.18	6.758
0	23	0	36.603

1	41	6.43	6.512
1	49	5.38	5.439
3	76	10.41	6.13
4	100	10.55	5.382
2	84	6.28	4.495
2	30	17.57	12.834
4	85	12.41	6.352
1	23	11.46	11.711
5	120	10.99	5.019
3	102	7.76	4.546
4	76	13.87	7.122

G. Sample 06CD16

Table S7.1 Data inputs for 06CD16

Sample #	Elev. (m)	Unit + Deposition Age (Ma)	Systems used
06CD16	0	Honna Formation* 95±5	AHe

*Lewis et al., 1991

Table S7.2 Thermal history constraints for model for 06CD16

Range for Time (Myr) general prior	Range for Temp (˚C) general prior	Geologic unit and depositional or emplacement age	Present Day Surface Temp (˚C)	Max. ∂T/∂t (˚C/Myr)
12.63 ± 12.63*	70 ± 70	--	10 ± 0	1000

*oldest single grain age

Table S7.3 Apatite and zircon-helium inputs 06CD16

Raw Date (Ma)	Error	eU (ppm)	Grain length (microns)	Grain width (microns)	Grain thickness (microns)
Sample 06CD16 (apatite)					
12.63	0.41	6.26	130	77	68
10.08	0.32	8.54	130	67	63
9.51	0.25	30.37	136	67	63
8.6	0.35	7.73	116	54	57
6.6	0.25	13.08	124	78	54
10.98	0.35	8.26	148	57	54
7.97	0.26	11.9	161	58	57
8.08	0.24	18.58	196	68	54
7.18	0.24	8.1	117	69	61

H. Sample 07CD16

Table S8.1 Data inputs for 07CD16

Sample #	Elev. (m)	Unit + Deposition Age (Ma)	Systems used
07CD16	0	Yakoun Formation* 170±5	AHe

*Lewis et al., 1991

Table S8.2 Thermal history constraints for model for 07CD16

Range for Time (Myr) general prior	Range for Temp (˚C) general prior	Geologic unit and depositional or emplacement age	Present Day Surface Temp (˚C)	Max. ∂T/∂t (˚C/Myr)
19.24 ± 19.24*	70 ± 70	--	10 ± 0	1000

*oldest single grain age

Table S8.3 Apatite and zircon-helium inputs 07CD16

Raw Date (Ma)	Error	eU (ppm)	Grain length (microns)	Grain width (microns)	Grain thickness (microns)
Sample 07CD16 (apatite)					
9.5	0.95	1.45	130	77	68
15.19	0.62	1.45	129	67	63
11.31	1.18	1.31	136	63	52
13.2	0.67	1.37	116	57	54
15.29	1.05	1.06	148	57	54
10.98	0.82	1.47	161	58	57
15.05	0.64	1.14	196	68	54
16.96	1.15	1.27	216	109	99
19.24	0.68	1.2	159	62	54

I. Sample 29CD16

Table S9.1 Data inputs for 29CD16

Sample #	Elev. (m)	Unit + Emplacement Age (Ma)	Systems used
29CD16	0	Honna Formation* 95±5	AHe

*Lewis et al., 1991

Table S9.2 Thermal history constraints for model for 29CD16

Range for Time (Myr) general prior	Range for Temp (˚C) general prior	Geologic unit and depositional or emplacement age	Present Day Surface Temp (˚C)	Max. ∂T/∂t (˚C/Myr)
12.05 ± 12.05*	70 ± 70	--	10 ± 0	1000

*oldest single grain age

Table S9.3 Apatite and zircon-helium inputs 29CD16

Raw Date (Ma)	Error	eU (ppm)	Grain length (microns)	Grain width (microns)	Grain thickness (microns)
Sample 29CD16 (apatite)					
9.18	0.24	45.94	116	57	54
7.96	0.36	5.85	161	58	57
7.5	0.45	4.76	117	69	61
10.97	0.54	3.78	159	62	54
10.99	0.43	5.04	149	69	61
12.05	0.38	7.3	149	69	61

5. QTQt model results

Below, we present results from QTQt models. For all samples, we show temperature probability heat map over the time which our data provides constraint. Hotter colors indicate higher probability for a given time-temperature point. Probability plot shows 95% credibility interval, shown by black lines enveloping time-temperature path, the model that best fits posterior probability (in olive), the best-fit single time-temperature path (maroon), weighted mean (black), and mode (white) results. We also provide a predicted vs. observed age plot for each model.

Barry Inlet Vertical Transect

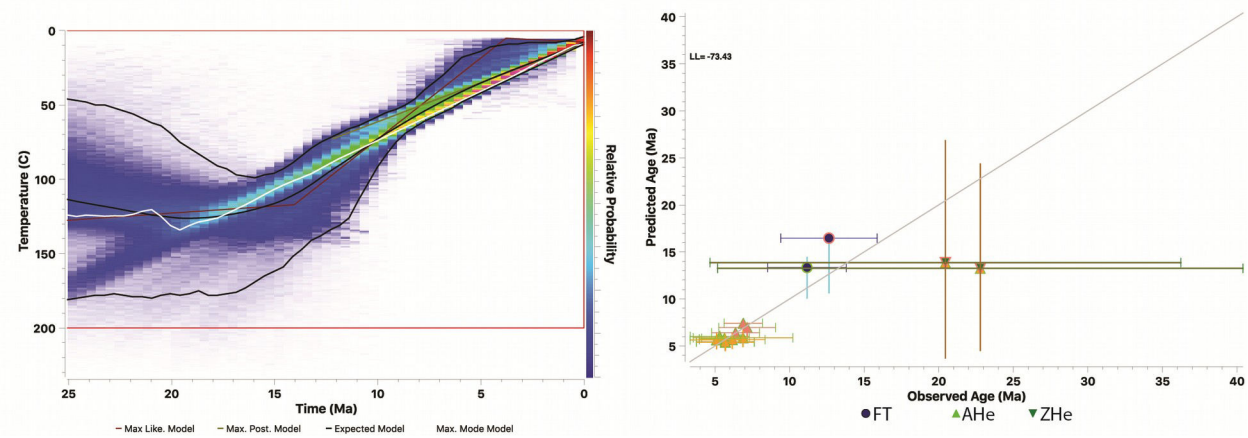

Figure S1. Time-temperature probability plot for sample HG04, the lowest sample in Barry Inlet Vertical Transect as well as predicted vs. observed age plot for model run.

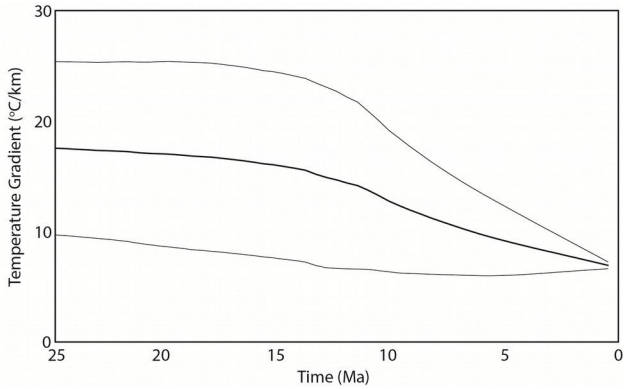

Figure S2. Estimated geothermal gradient for Barry Inlet Vertical Transect. Predicted geothermal gradient of ~20°Ckm^{-1} agrees well with our chosen gradient for exhumation estimates.

HG02

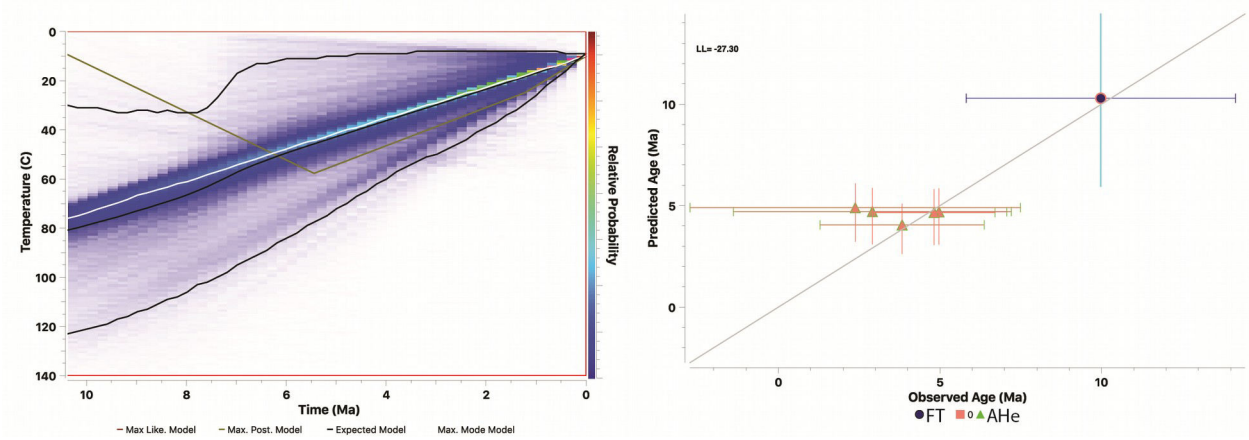

Figure S3. Time-temperature probability plot for sample HG02 as well as predicted vs. observed age plot for model run.

HG12

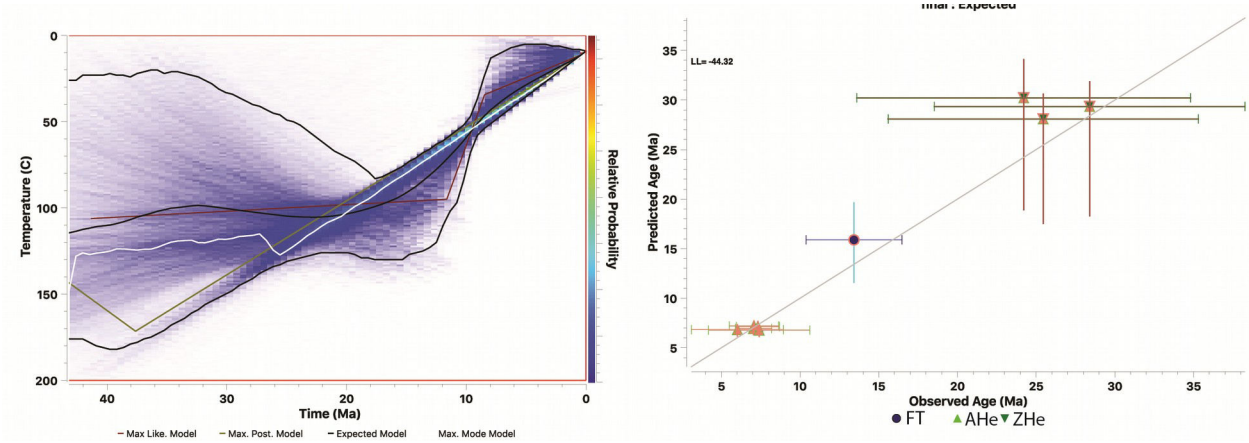

Figure S4. Time-temperature probability plot for sample HG12 and predicted vs. observed age plot for final model run.

HG19

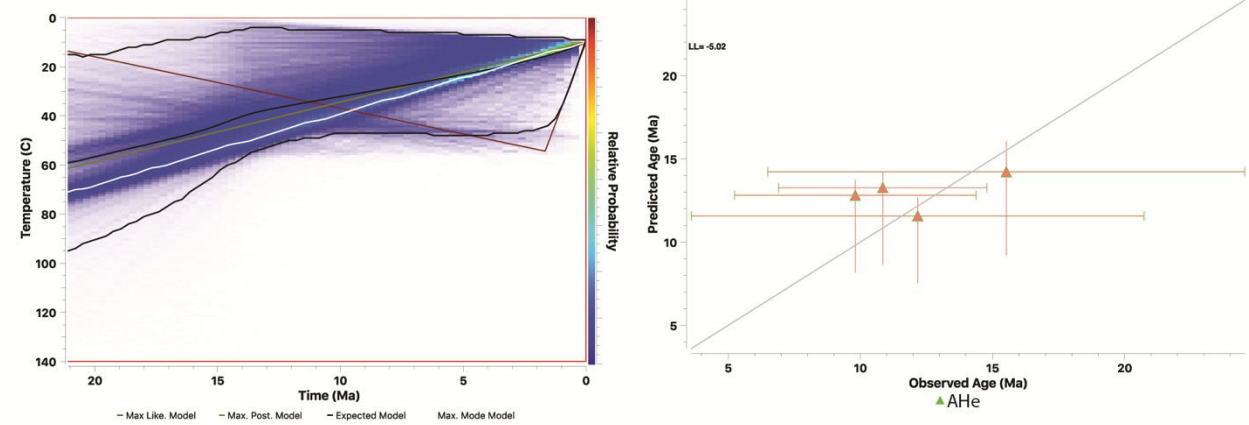

Figure S5. Time-temperature probability plot for sample HG19 and predicted vs. observed age plot for final model run.

HG28

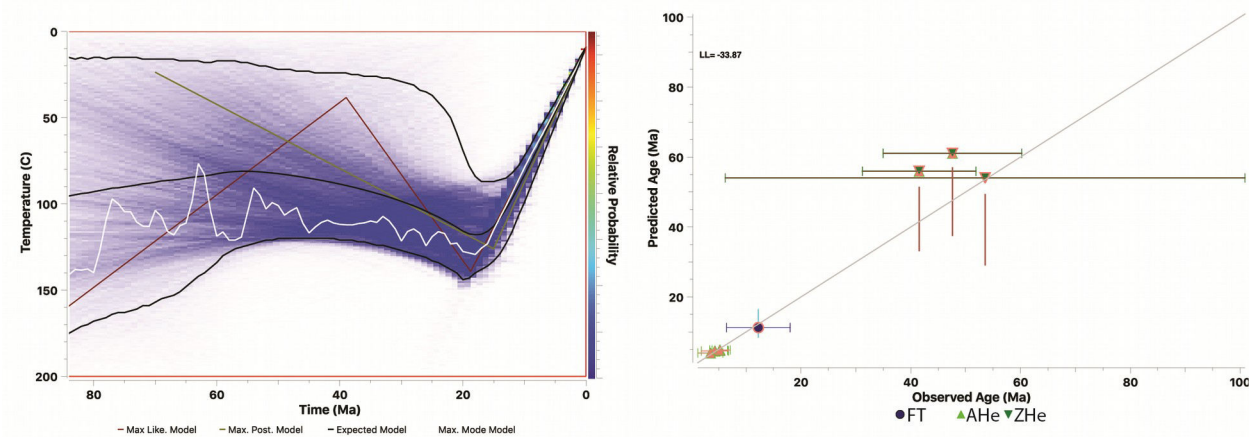

Figure S6. Time-temperature probability plot for sample HG28 and predicted vs. observed age plot for final model run.

HG34

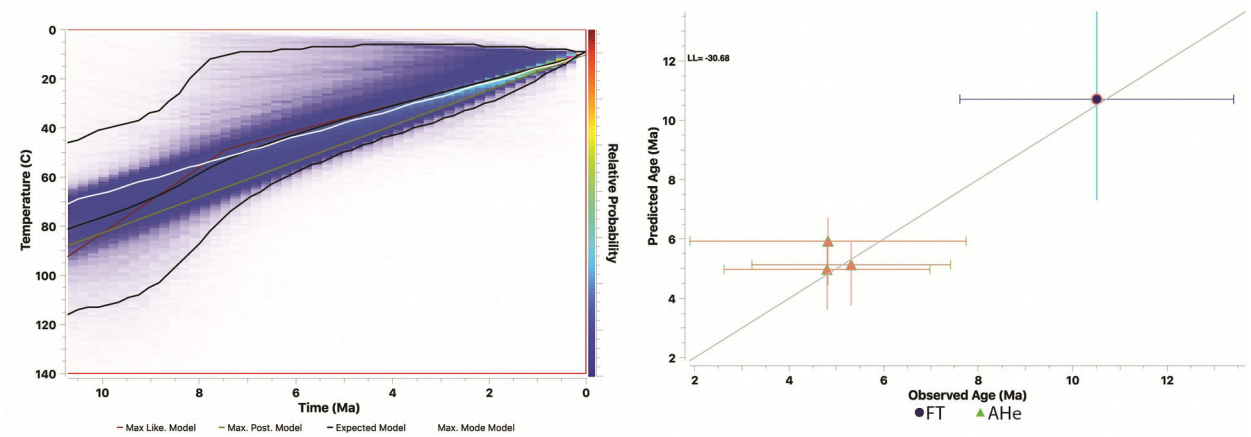

Figure S7. Time-temperature probability plot for sample HG34 and predicted vs. observed age plot for final model run.

06CD16

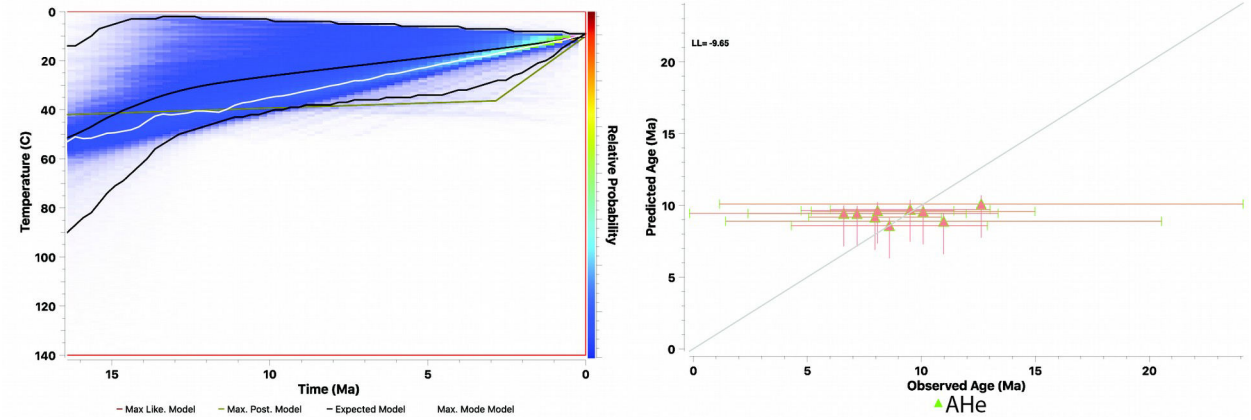

Figure S8. Time-temperature probability plot for sample 06CD16 and predicted vs. observed age plot for final model run.

07CD16

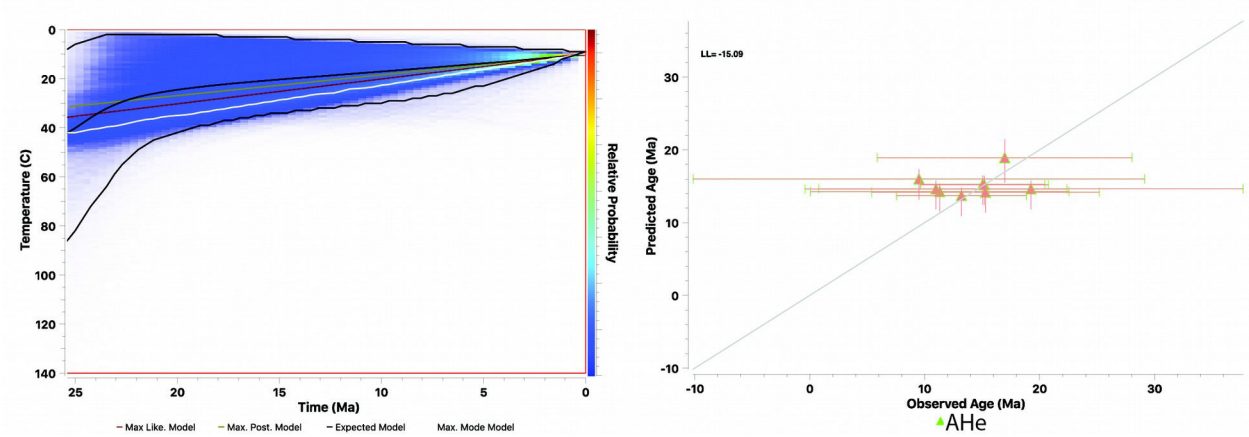

Figure S9. Time-temperature probability plot for sample 07CD16 and predicted vs. observed age plot for final model run.

29CD16

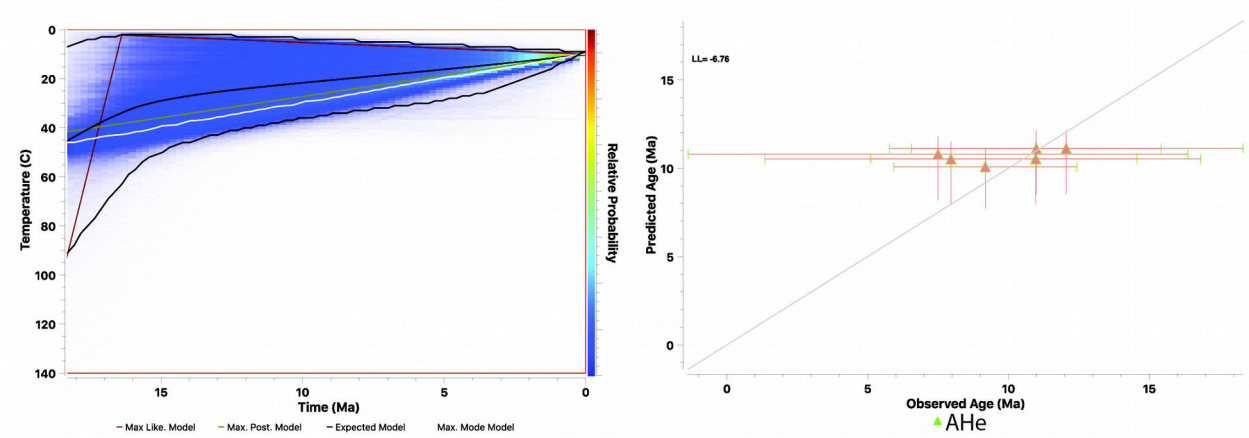

Figure S10. Time-temperature probability plot for sample 07CD16 and predicted vs. observed age plot for final model run.

6. Sample dates relative to distance from plate margin

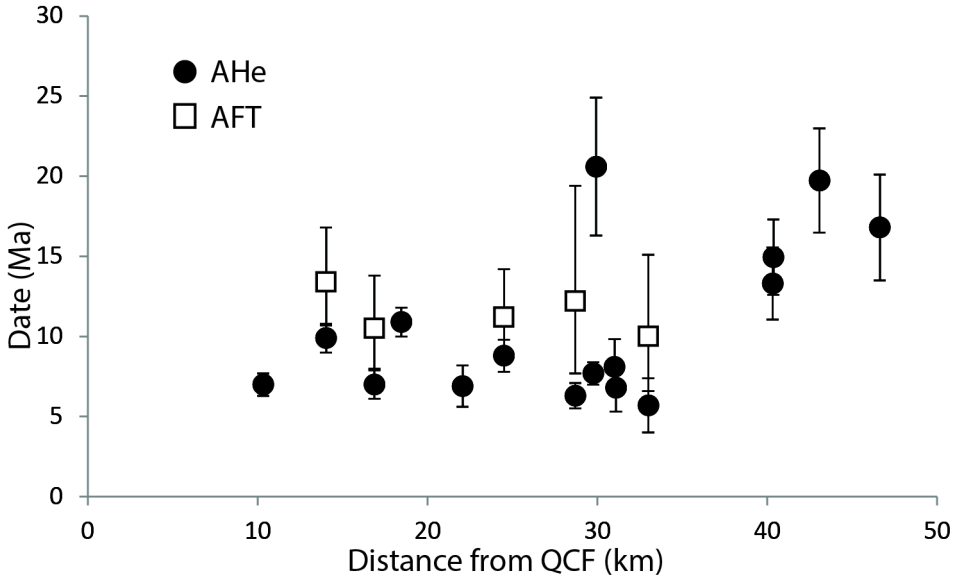

Figure S11. AHe and AFT dates relative to distance from the Queen Charlotte Fault. AHe dates less than 30-40 km distance from the Queen Charlotte Fault are younger than those found to the east.

7. Plate motion reconstruction of Yakutat terrane and Pacific plate relative to North America

SV1. Animation of Pacific plate motion relative to stable North America using Demets & Merkoureiv (2016) kinematic model. Yakutat terrane is assumed to move with Pacific plate.

SV2. Animation of Pacific plate motion relative to stable North America using Doubrovine & Tarduno (2008) kinematic model. Yakutat terrane is assumed to move with Pacific plate.

To better understand the tectonic history of Haida Gwaii, we reconstruct relative plate motions between the Pacific and North American plates using the kinematic models of Demets & Merkouriev (2016) and Doubrovine & Tarduno (2008), with the tectonic reconstruction software Gplates (Müller et al., 2018). The Demets & Merkouriev (2016) kinematic model resolves plate motion to ~20 mya in high resolution (~1 myr) increments whereas Doubrovine & Tarduno (2008) resolves plate motion to the Cretaceous albeit at much lower resolution. We chose to limit our reconstruction to the past 25 myr because the Yakutat terrane is predicted to have moved with the Pacific plate relative to stable North America since this time (Plafker 1987; Hyndman & Hamilton 1993). Results were used to make figure 4 in the main text as well as two supplemental videos showing plate motion for each kinematic model (SV1 and SV2).

Plate reconstruction using Demets & Merkouriev (2016) and Doubrovine and Tarduno (2008) rotations show only subtle distinctions (SV1, SV2). Below, we review first-order observations from these models as presented by previous workers. We also present new observations that synthesize regional geology with plate motions.

First, the track of the south-east corner of the Yakutat terrane is roughly consistent with the trace of the Queen Charlotte Fault (SV1, SV2). This observation led previous workers to suggest that most intraplate convergence following the passage of the Yakutat terrane was not taken up by shortening of the North American plate (Demets & Merkouriev 2016) and that terrane translation led to strain localization at the ocean-continent boundary (Ten Brink et al., 2018). North of Haida Gwaii, the flowpath of the Yakutat terrane deviates by a maximum of 35 km west from the plate boundary as defined by the Queen Charlotte Fault. This deviation steadily decreases to the north, until the plate boundary and Yakutat flowpath are in tandem again off northern Baranoff Island. Assuming this offset is due to deformation of the North American plate following passage of the Yakutat terrane, ~ 4 km/myr eastward motion of the Queen Charlotte Fault relative to stable North America is estimated. This rate is similar in magnitude to the ~5±2 mm/yr long-term shortening of North America predicted from gps residuals in the northern Queen Charlotte Basin (Mazzotti et al., 2003).

A second observation is that, projected back to 25 mya, the Yakutat terrane lies adjacent northern Vancouver island, with the south-eastern portion of the terrane offshore Brooks Peninsula (SV2; Fig. 4, main text). Previous work suggests the Brooks Peninsula was the locus of the Pacific, North America, Juan de Fuca triple junction from 40 mya up to ~2-8 mya (Botros & Johnson, 1988; Lewis et al., 1997; Rohr & Tryon 2010). The juxtaposition of the Yakutat terrane against this purported plate boundary lends credence to the hypothesis that the terrane only became coupled with the Pacific plate 25 mya (Plafker, 1987). A change in Pacific plate motion relative

to the Hawaii hotspot ~25 mya (Jicha et al., 2018), may be linked to transfer of the Yakutat terrane to the Pacific plate and the beginning of northward translation of the terrane from the triple junction.

Finally, estimates of total underthrusting of Pacific plate vary significantly if it is assumed underthrusting begins at the Brooks Peninsula vs. the Tuzo Wilson Seamounts (SV1, SV2). These projections result in either ~50 km or ~120 km underthrusting at the location of the 2012 Haida Gwaii earthquake. Assuming underthrusting began at the Tuzo Wilson Seamounts, the plate overlap encompasses the region of elevated topography on Haida Gwaii, as previously noted by Ten Brink et al., (2018) (Sv1, SV2). Our results do not provide constraint on which of these scenarios is correct. Interestingly, the trace of this underthrust extent also closely follows that of the western-most coastline on Prince of Wales island and the Alexander Archipelago. Whether this is a coincidence or due to along-strike differences in upper plate response to underthrusting is unknown.

Previous studies emphasize predictions from Pacific-North America relative plate motion models that convergence rates have increased since the Miocene along the southern Queen Charlotte Fault adjacent Haida Gwaii (Rohr et al., 2000; Hyndman 2015; ten Brink et al., 2018). In figure S12 we show predicted convergence rates, obliquity and net shortening since 20 mya using the most recently published Pacific-North America relative plate motion model (Demets & Merkouriev, 2016), for the Queen Charlotte Fault in southern, central, and northern Haida Gwaii (Fig. 2, A, B, C, main text). Additionally, we plot the predicted timing of subduction initiation given a critical convergence obliquity of 15^{o} CW from the local strike of the Queen Charlotte Fault, as well as the timing of passage of the south-eastern part of the Yakutat Terrane.

Results are consistent with previous studies examining relative plate motion in this region (Demets & Merkouriev, 2016; ten Brink et al. 2018). The northern (A) sample location experienced an ~8 myr phase of transtension prior to transpression beginning ~11 mya. The Central (B) sample location experienced a less significant phase of transtension prior to transpression beginning ~13 mya. The southern (C) location is predicted to have experienced transpression for the past 20 myr. Total intraplate shortening since the Miocene decreases from 160 to 90 km from south to north (C to A).

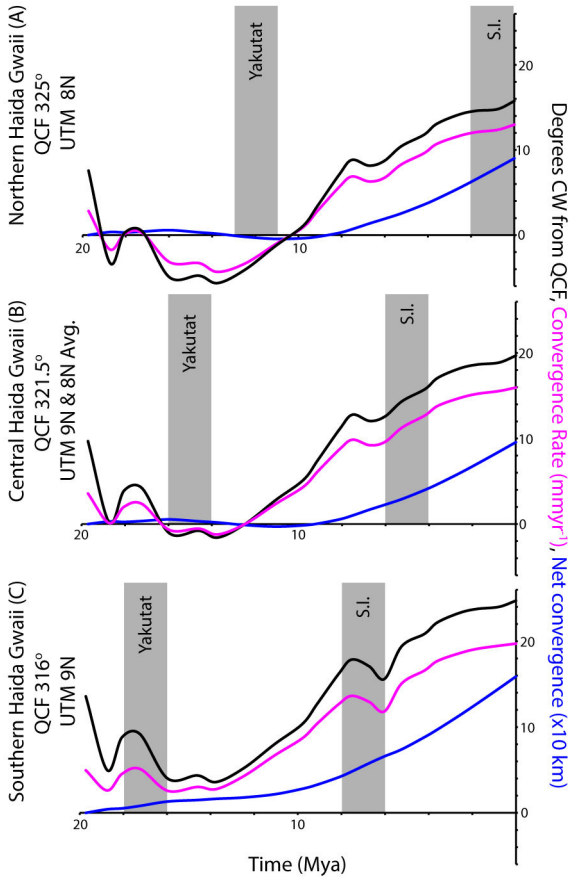

Figure S12. Convergence rate, convergence obliquity, and net convergence for sites A, B, C from Figure 2 in the main text, calculated from the best-fit angular velocities for Pacific-North America plate motion from Demets & Merkouriev (2016). Local Queen Charlotte Fault azimuth measured in ArcGIS in UTM zone 9N and 8N projections. Yakutat passage timing from Demets & Merkouriev (2016). Potential subduction initiation (S.I.) is taken to occur at a critical convergence obliquity of 15° (Trehu et al., 2015; ten Brink et al., 2018).

References

Botros, M., Johnson, H.P., 1988, Tectonic evolution of the Explorer-northern Juan de Fuca region from 8 Ma to the present: Journal of Geophysical Research, 93 p 10,421-10,437

Brandon, M.T., 2002, On Track, v. 24, p. 13-18.

Brothers, D.S., Miller, N.C., Barrie, J.V., Haeussler, P.J., Greene, H.G., Andrews, B.D., Zielke, O., Watt, J., Dartnell, P., 2020, Plate boundary localization, slip-rates and rupture segmentation of the Queen Charlotte Fault based on submarine tectonic geomorphology: Earth and Planetary Science Letters v. 530

Demets, C., Merkouriev., 2016, High-resolution reconstructions of Pacific-North America plate motion: 20 Ma to present: Geophysical Journal International, v. 207, p. 741-773

Doubrovine, P.V., Tarduno, J.A., 2008, A revised kinematic model for the relative motion between Pacific oceanic plates and North America since the late Cretaceous: Journal of Geophysical Research Solid Earth v. 113:B12101

Dumitru, T.A., 1993, A new computer automated microscope stage system for fission-track analysis: Nuclear Tracks and Radiation Measurements, v. 21, p. 575–580.

Flowers, R.M., Ketcham, R.A., Shuster, D.L., Farley, K.A., 2009, Apatite (U-Th)/He thermochronometry using a radiation damage accumulation and annealing model: Geochimica et Cosmochimica Acta, v. 73, no. 8

Galbraith, R.F., 1981, On statistical methods of fission track counts: Mathematical Geology, v. 13, p. 471–478.

Gallagher, K., 2012, Transdimensional inverse thermal history modeling for quantitative thermochronology: Journal of Geophysical Research: Solid Earth, v. 117, no. B2

Green, P.F., 1981, A new look at statistics in fission track dating: Nuclear Tracks, v. 5, p. 77–86.

Guenthner, W.R., Reiners, P.W., Ketcham, R.A., Nasdala, L., Giester, G., 2013, Helium diffusion in natural zircon: Radiation damage, anisotropy, and the interpretation of zircon (U-Th)/He thermochronology: American Journal of Science, v. 313, no. 3

Hurford, A.J., and Green, P.F., 1983, The Zeta age calibration of fission-track dating: Isotope Geoscience, v. 1, p. 285–317.

Hyndman, R.D., Hamilton, T.S., 1993, Queen Charlotte area Cenozoic tectonics and volcanism and their association with relative plate motions along the northeastern Pacific margin: Journal of Geophysical Research, v. 98, no. B8, p. 14,257-14,277

Hyndman, R., 2015 Tectonics and structure of the Queen Charlotte Fault Zone, Haida Gwaii, and large thrust earthquakes: Bulletin of the Seismological Society of America, v. 104, no. 2B

Jicha, B.R., Garcia, M.O., Wessel, P., 2018, Mid-Cenozoic Pacific plate motion change: Implications for the northwest Hawaiian Ridge and circum-Pacific: Geology, 46:11

Ketcham, R.A., Gautheron, C., Tassan-Got, L., 2011, Accounting for long alpha-particle stopping distances in (U-Th-Sm)/He geochronology: Refinement of the baseline case: Geochimica et Cosmochimica Acta, v. 75, no. 24

Lewis, T.J., Lowe, C., Hamilton, T.S., 1997, Continental signature of a ridge-trench-triple junction: Northern Vancouver Island: Journal of Geophysical Research, 102:B4

Lewis, P.D., Haggart, J.W., Anderson, R.G., Hickson, C.J., Thompson, R.I., Dietrich, J.R., Rohr, K.M.M., 1991, Triassic to Neogene geologic evolution of the Queen Charlotte region: Canadian Journal of Earth Sciences, v/ 28 p. 854-869

Mazzotti, S., Hyndman, R.D., Fluck, P., Smith, A.J., Schmidt, M., 2003, Distribution of the Pacific/North America motion in the Queen Charlotte Islands-S. Alaska plate boundary zone: Geophysical Research Letters, v. 30, no. 14

Müller, R. D., Cannon, J., Qin, X., Watson, R. J., Gurnis, M., Williams, S., et al. 2018. GPlates: Building a virtual Earth through deep time. Geochemistry, Geophysics, Geosystems, 19. doi:10.1029/2018GC007584.

Naeser, C.W., 1979, Fission track dating and geologic annealing of fission tracks: *in* Jager, E., and Hunziker, J.C., eds., Lectures in Isotope Geology, Springer-Verlag, Berlin, p. 154-169.

Plafker, G., 1987, Regional geology and petroleum potential of the northern Gulf of Alaska continental margin, in Scholl, D.W., Grantz, A., and Vedder, J.G., eds., Geology and Resource Potential of the Continental Margin of Western North America and Adjacent Ocean Basins, Beaufort Sea to Baja California, Volume 6: Houston, Texas, Circum-Pacific Council for Energy and Mineral Resources, p. 229–268.

Rohr, K.M.M., Scheidhauer, M., Trehu, A.M., 2000, Transpression between two warm mafic plates: the Queen Charlotte Fault revisited: Journal of Geophysical Research, v. 105, no. B4

Rohr, K.M.M, Tryon, A.J., 2010, Pacific-North America plate boundary reorganization in response to a change in relative plate motion: Offshore Canada: Geochemistry Geophysics Geosystems v. 11, no. 6

ten Brink, U.S., Miller, N.C., Andrews, B.D., Brothers, D.S., Haeussler, P.J., 2018, Deformation of the Pacific/North America plate boundary at Queen Charlotte Fault: The possible role of rheology: Journal of Geophysical Research, Solid Earth, v. 123, no. 5

Trehu, A.M., Scheidhauer, M., Rohr, K.M.M., Tikoff, B., Walton, M.A.L., Gulick, S.P.S., Roland, E.C., 2015, An abrupt transition in the mechanical response of the upper crust to transpression along the Queen Charlotte Fault: Bulletin of the Seismological Society of America, v. 104, no. 2B